Available online at www.sciencedirect.com

ScienceDirect

Russian Geology and Geophysics 57 (2016) 1349–1358

RUSSIAN GEOLOGY AND GEOPHYSICS

www.elsevier.com/locate/rgg

Interpretation of shallow electrical resistivity images of faults: tectonophysical approach

K.Zh. Seminsky [a,*], R.M. Zaripov [a], V.V. Olenchenko [b,c]

[a] *Institute of the Earth's Crust, Siberian Branch of the Russian Academy of Sciences, ul. Lermontova 128, Irkutsk, 664033, Russia*
[b] *A.A. Trofimuk Institute of Petroleum Geology and Geophysics, Siberian Branch of the Russian Academy of Sciences, pr. Akademika Koptyuga 3, Novosibirsk, 630090, Russia*
[c] *Novosibirsk State University, ul. Pirogova 2, Novosibirsk, 630090, Russia*

Received 1 April 2015; accepted 28 August 2015

Abstract

A new approach to interpretation of shallow electrical resistivity tomography (ERT) data discussed for the case of the Olkhon area (western Baikal region) stems from tectonophysical ideas of faulting phases and deformation levels in rocks. The deformation levels, identified statistically from ERT responses, constrain fault boundaries and subboundaries associated with the formation of main and subsidiary fault planes. Information of this kind creates a basis for solving various fundamental and applied problems of tectonics, mineral exploration, and engineering geology.

Keywords: fault zone; shallow electrical resistivity tomography

Introduction

Resistivity imaging (Bobachev et al., 1995; Griffiths and Barker, 1993) or electrical resistivity tomography (ERT), an updated version of vertical electrical soundings (VES), has been largely used to study faulting in shallow crust to depths of 40 m (Carbonel et al., 2013; Improta et al., 2010; Kuria et al., 2010; Magnusson et al., 2010; Olenchenko and Kamnev, 2014; Ryazantsev, 2012; Schutze et al., 2012; Sokolov et al., 2011). ERT data are interpreted proceeding from known correlations between resistivity and lithology. Faults presumably correspond to zones of resistivity gradients or to centers of linear low-resistivity zones, but this interpretation fails in areas of complex deformation patterns unless *a priori* data is used and/or the results are checked against other geophysical data.

The ways in which faults show up in ρ variations are identified by means of 2D resistivity modeling (mapping) and inversion of ERT responses of heavily deformed rocks (Reiser et al., 2009; Ronning et al., 2014). Research in this line can reveal a set of formal diagnostic features of faults in resistivity sections, but the problem is that faults are heterogeneous geological bodies producing intricate resistivity patterns.

In terms of tectonophysics, a fault zone consist of a main plane delineated by tectonites and smaller subsidiary faults and fractures of different ranks. A complete cycle of faulting consists of three successive phases, without the elastic or ductile prefracture phase (Seminsky, 2003, 2014; Seminsky et al., 2013). Faulting begins within a broad zone of small genetically related fractures called a "fracture zone", a "zone of incipient faulting", etc. (Favorskaya et al., 1985; Khrenov, 1971; Makarov and Shchukin, 1979; Peive, 1990; Radkevich et al., 1956; Rats and Chernyshev, 1970). Then the zone of active faulting narrows down and strongly deformed rocks separate several small fragments of the main fault plane. Finally, at the phase of ultimate failure, a fault becomes a single main plane surrounded by large pinnate faults filled with soft tectonites (fault gouge, breccia, etc.).

Structures that arise during different phases of deformation are superposed one upon another producing transverse subzones within the damage area (Fig. 1) corresponding to three phases of ultimate failure (I) and late (II) and early (III) faulting, grading one to another off the fault axis. This zoning records different deformation levels in rocks, which are expected to show up in resistivity patterns controlled by water-filled porosity and cracks of different sizes.

* Corresponding author.
E-mail address: seminsky@crust.irk.ru (K.Zh. Seminsky)

1068-7971/$ - see front matter
http://dx.doi.org/10.1016/j.rgg.2016.08.020

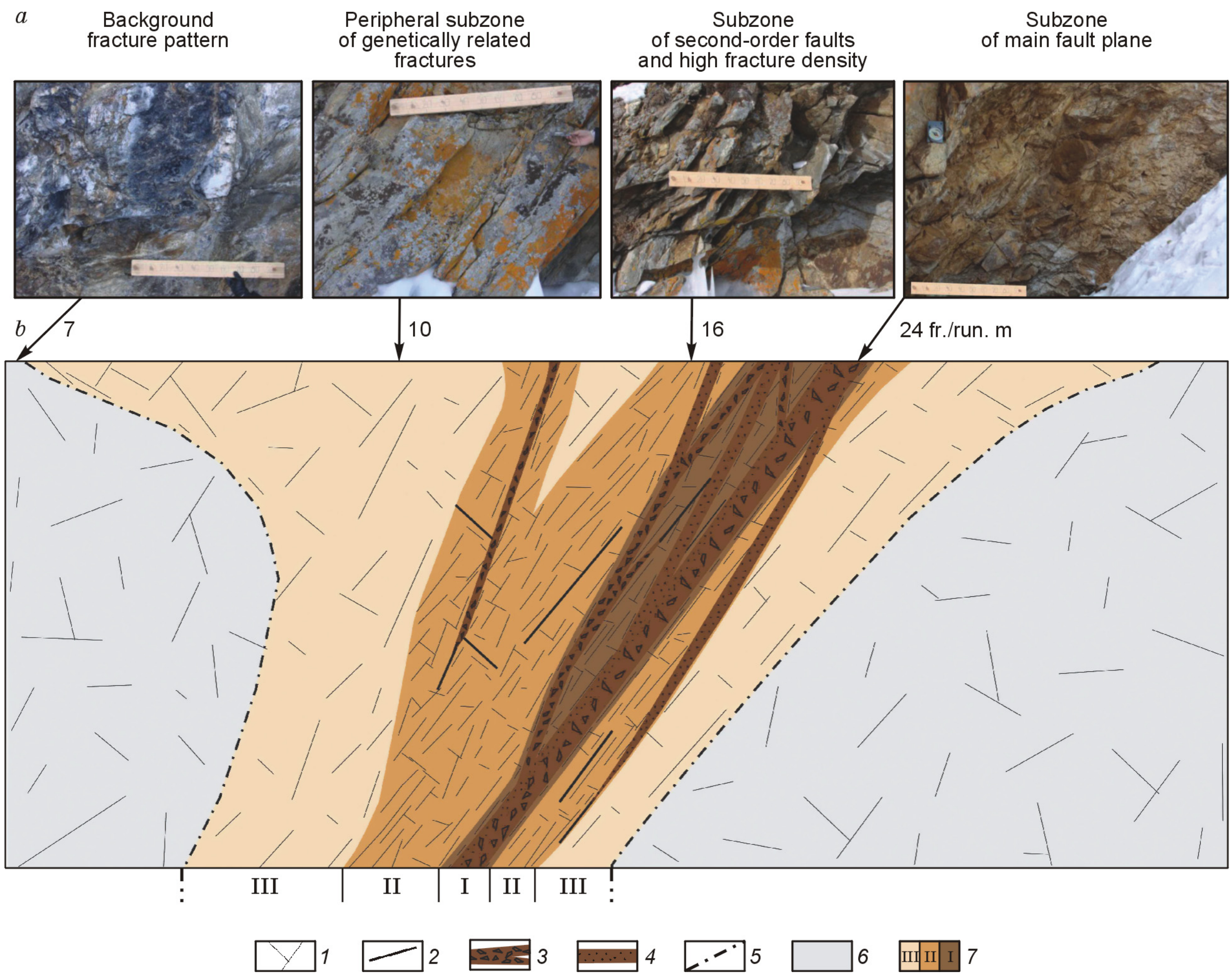

Fig. 1. Cross section of a fault zone: a basic model. *a*, Photographs illustrating typical facture patterns near the main fault plane at a site in the Olkhon area, Western Baikal region (scale bar is 1 m). *b*, transverse zoning of a fault that underwent three evolution phases. *1*, fracture pattern; *2*, large fractures; *3*, fault plane filled with breccia material; *4*, fault plane filled with gouge material; *5*, fault zone boundary; *6*, weakly deformed rocks; *7*, basic elements of fault zone formed during different phases of faulting: peripheral subzone of genetically related fractures (III); subzone of second-order faults and high fracture density (II); subzone of main fault plane (I).

In this study we report principles of a tectonophysical approach to interpretation of resistivity images of active tectonic areas. The specific objectives include (1) collecting resistivity images of reference faults in the Olkhon area (Western Baikal region) documented previously by structural methods; (2) processing ERT responses of shallow crust and correlating them with faulting patterns; (3) explaining the ERT data processing results in terms of the tectonophysical theory and justifying their use as markers of boundaries and subboundaries of fault zones.

Objects and methods

The Olkhon area in the western Baikal region (Fig. 2) belongs to an uplifted margin of the Sayan–Baikal fold belt. It comprises metamorphic complexes of different ages with nearly vertical bedding. The rocks underwent several major events of post-Proterozoic deformation (Delvaux et al., 1995, 1997; Levi et al., 1997; Logatchev, 2003; Makrygina et al., 2014; Mats, 1993; Seminsky et al., 2013; Sherman et al., 1992, 1994; Sklyarov, 2005; Zamaraev et al., 1979; etc.): Early Paleozoic compression, Early Cenozoic shear, and Late Cenozoic extension. The deformation shows up as a dense network of faults and fractures, with motions along them maintaining the NW–SE extension associated with the Cenozoic Baikal rifting.

ERT responses were collected from steep faults bordering large and small Cenozoic basins, at eleven sites (Fig. 2). The faults that were documented previously by direct structural measurements at most of the sites within Lake Baikal coastal cliffs (10, 11, 13, 15, 17, and 19) were used for reference. In other cases (sites 12, 14, 16, 18, and 20), the presence of faults was inferred from geomorhically expressed scarps presumed to correspond to fault planes. Some of them were large faults, such as the Primorsky and Tyrgan–Kuchelga normal faults bordering the Buguldeika–Chernorud graben (Fig. 2).

The sites with reference faults were chosen such that their resistivity patterns could be controlled mostly by deformation, the lithology control being excluded wherever possible. Those were faulted sites 10, 11, 13, 15, 17, and 19 located outside the Chernorud tectonic zone where conducting graphite produced low-resistivity belts (Kozhevnikov, 1998). Other prerequisites were the lack of soft sediments interfering with bedrock responses and frozen ground producing high-resistivity anomalies; to avoid the latter effect, all measurements were run in the summer time.

Deformation was studied by ERT and structural measurements along profiles. The sites of reference faults were located most often above high bedrock outcrops or cliffs (as far as the pebble beach) which could provide geological constraints. That was the case of site 15 at the Ontkhoi Cape (Fig. 2) where the relations between resistivity and faulting patterns were the most obvious (Fig. 3).

Structural measurements at reference sites (Fig. 3*b*) were supposed to reveal styles of deformation by faults of different ranks in main lithologies: granites, granite gneisses and gneisses of various other types, marbles, as well as mylonites, cataclastics, etc. from Precambrian fault zones. The Precambrian zones of weakness accommodated stress and released it during later tectonic events which produced faults oriented in the NE (Baikal) direction at most of the sites (Fig. 3*b*, *c*). They appear in the surface topography as depressions (Fig. 3*a*) resulting from erosion and weathering of the deformed bedrock.

Some relatively large fault planes in bedrock exposures are marked by breccias or fault gouge, up to several centimeters thick in bulges. The spatial variations of deformation degrees along the profiles of structural measurements were presented as density *D* of fractures, or their number per running meter measured at equal spacing; *D* highs correlated with large faults in the reference zones (Fig. 3*c*). Normal slip in NE faults revealed by tectonophysical reconstructions with the methods of Gzovsky (1975) and Nikolaev (1992), along with distinct geomorphic expression, evidence of their activity during the Late Cenozoic rifting.

The obtained resistivity maps imaged shallow crust to depths 40–50 m or were high-resolution images of the upper 10 m (Fig. 3*d*) or 5 m, depending on the electrode spacing. The techniques of data acquisition and processing were developed and tested in the course of previous surveys in the Western Baikal region (Zaripov, 2013). ERT responses were collected by a *Skala-48* multielectrode station, with the configuration of electrodes like in symmetrical Schlumberger systems with a spacing of 0.5, 1, and 5.0 m. The acquired ERT data were inverted using *Res2DInv* software (Loke, 2010). Altogether, several tens of resistivity maps were obtained along profiles varying in length from 70 to 5000 m depending on the required resolution and fault sizes.

The recorded resistivities vary from a few Ohm·m to tens of thousand Ohm·m (Fig. 3*d*) as a function of deformation degree and water content in rocks. The near-surface (1.5–2.0 m) parts of sections in capes are dry aeration zones in summer, with resistivity as high as 2000 to 10,000 Ohm·m, while the resistivity of rocks below these depths records more faithfully the deformation and moisture patterns. Strongly deformed zones appear as low-resistivity anomalies (a few

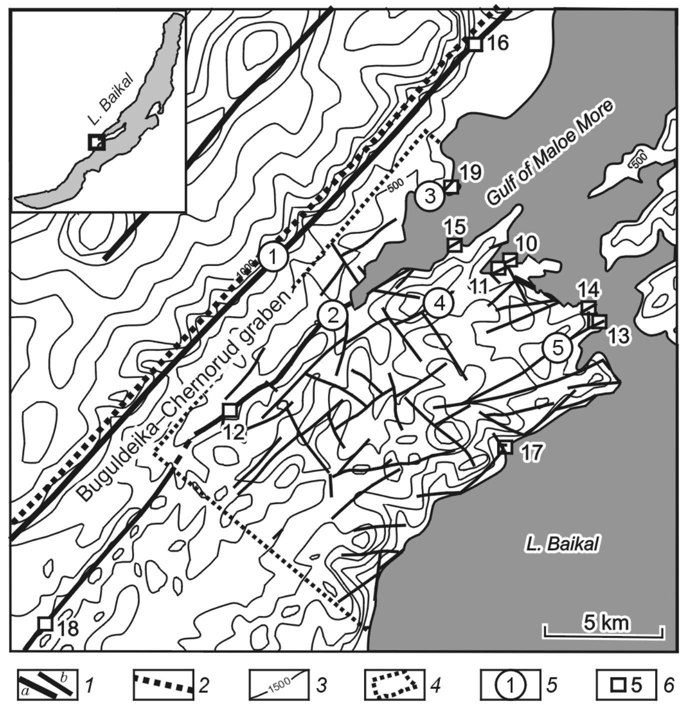

Fig. 2. Location map of faults and sites of resistivity imaging and structural measurements in the Olkhon area, Western Baikal region. *1*, large (*a*) and small (*b*) faults; *2*, Siberian craton margin; *3*, topographic contour lines; *4*, site of structural measurements showing presence of faults (Seminsky, 2005); *5*, large faults of Olkhon area. Roman numerals stand for fault names: 1, Primorsky; 2, Tyrgan–Kuchelga; 3, Ulirba; 4, Kurkut; 5, Tutai; *6*, sites of studies and their numbers.

Ohm·m) produced by high water contents and clay-size weathering products, while less deformed blocks are more resistive (5000–7000 Ohm·m on average).

The spatial relations of low- and high-resistivity zones provide clues to locations of faults, but detecting faults in ERT responses requires respective criteria based on correlation between resistivity and deformation.

Correlation between fracture density and resistivity in bedrocks of the Olkhon area

The recorded resistivity values ρ were plotted against the fracture density *D* (Fig. 4) at reference sites, where structural and geophysical transects were correlated within profile intervals. The resistivity-fracture density relationship is exponential at the first approximation and agrees with predictions that even minor fractures in rocks increases their effective conductivity (Gubatenko et al., 2000). Natural rocks *in situ* become more conductive as fractures and voids in them grow and become filled with water or fine-grained products of weathering, which has been proven recently by geoelectrical imaging (Danielsen and Dahlin, 2009; Ganerod et al., 2006; Magnusson et al., 2010; Ronning et al., 2014). Thus, fracture density in the heavily faulted crust of the Olkhon area is a proxy of deformation degree which controls near-surface ρ patterns.

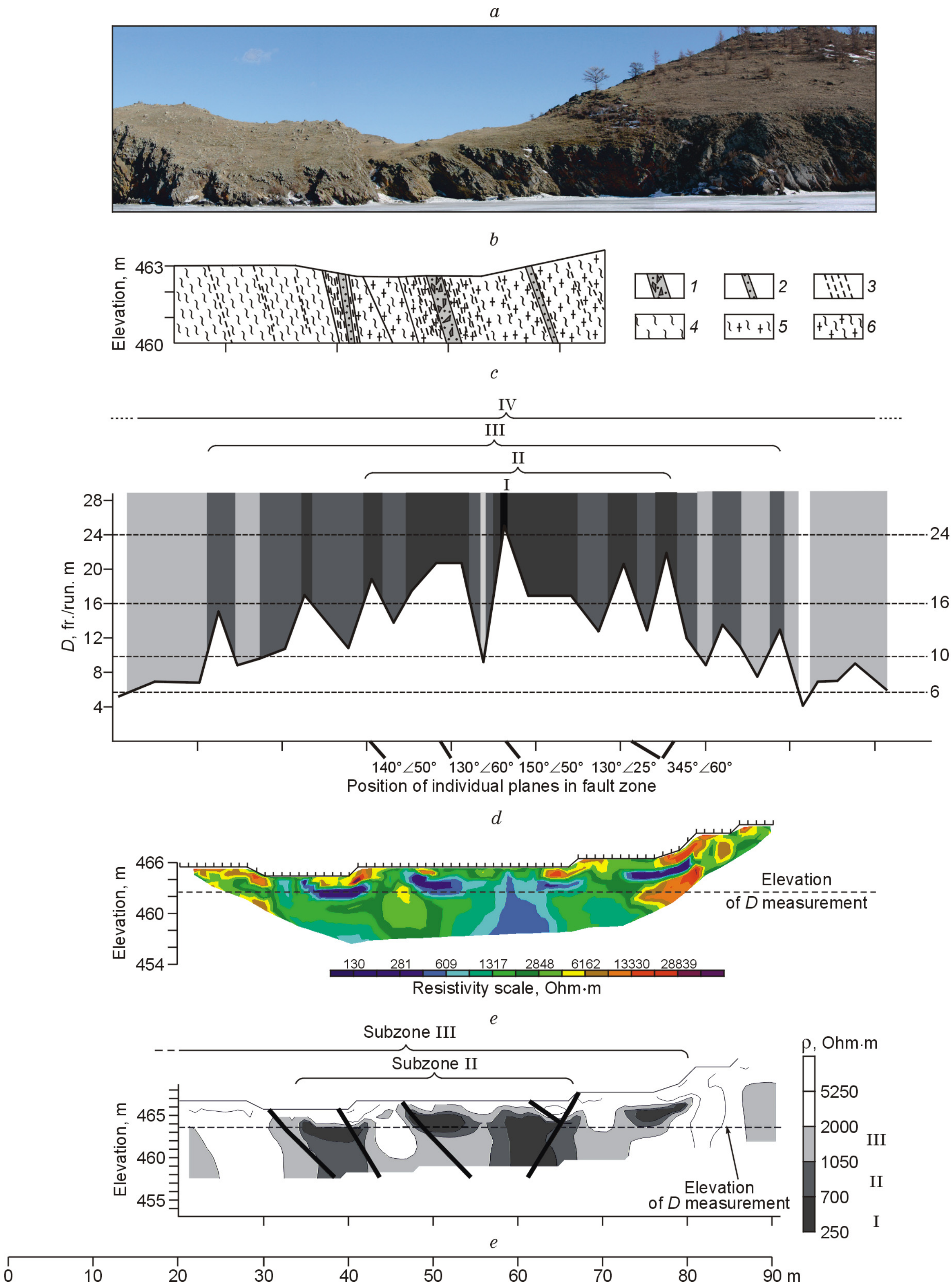

Fig. 3. Structural and ERT data from a reference fault zone in Ontkhoi Cape interpreted using the tectonophysical approach. *a*, Photograph of reference fault zone in Ontkhoi Cape expressed as several wave-cut caves and a topographic depression; *b*, structural cross section of cliffs in Ontkhoi Cape: *1*, *2*, fault planes marked by breccia (*1*) or fault gouge (*2*) material; *3*, heavily fractured bedrock outcrop; *4*, gneisses; *5*, granite gneisses; *6*, Precambrian mylonites; *c*, fracture density (*D*) variations along a profile. Gray and black shades show segments where fracture density exceeds four limit *D* values (dash lines). Braces above the curve are generalized boundaries of fragments corresponding to five levels of deformation (I to V) based on *D* distribution; heavy lines below show strike and dip of fault planes; *d*, *e*, resistivity sections along a profile above the Ontkhoi cliff, with standard contour lines (*d*) and with those according to statistically distinguished ρ levels (*e*). Braces above the curve are generalized boundaries of crust fragments corresponding to resistivity levels II and III; black lines are inferred positions of fault planes; *f*, distances along profile (for *b*–*e*).

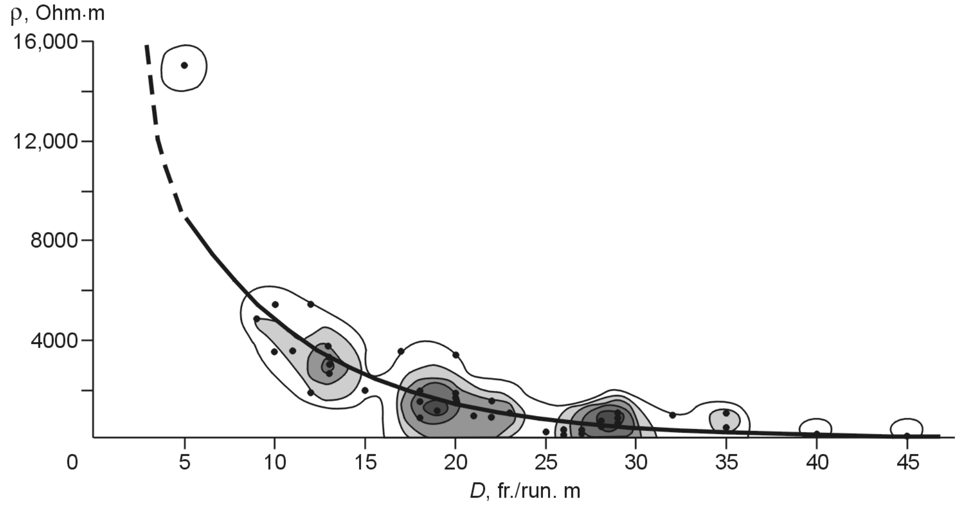

Fig. 4. Resistivity (ρ) vs. fracture density (D), from ERT data collected at 0.5 m electrode spacing in different rocks of Olkhon area. Contour lines illustrate uneven distribution of data points along the exponent curve.

Note that the data points are scattered relative to the approximation curve (Fig. 4). The contour lines of their density show four main peaks (without spike points) corresponding to deformation levels, with the respective ρ and D values. The patterns of the two parameters analyzed separately show the same regularity.

Fracture density (D) histograms (Fig. 5*a*) for reference sites include five levels (I–V) with approximately equal frequencies of D values, excluding a few spikes. The frequency is the highest at level III, while four other levels make up symmetrical pairs at the descending branches of the lognormal distribution. The five levels are better pronounced in the histogram of fracture density based on a larger sample of measured values (Fig. 5*b*). Average regional-scale D values that mark boundaries of deformation levels V to I at cape sites in the Olkhon area are, respectively, 4, 7, 16 and 25 fractures per running meter.

ERT data likewise show five levels (I–V) of ρ values, as in the case of the Ontkhoi site (Fig. 5*c*). The maximum resistivity corresponds to level III while the pairs of levels II, IV and I, V are located symmetrically on the descending branches of the lognormal normal ρ distribution. The ρ curve with increasing values at equal intervals along the x axis also comprises five segments (Fig. 5*d*) which are separated by kinks and approximated by lines with their slopes corresponding to the rates of resistivity increase. The slopes are the steepest within segments I and V, the shallowest within segment III represented by most frequent resistivity values for the faulted cliff at the Ontkhoi Cape, and intermediate within II and IV. The boundaries between ρ levels are the same in the histogram and in the curve for the Ontkhoi site (Fig. 5*c*, *d*), but this is not always the case at other sites.

The ρ patterns for different sites are of three main types (Fig. 6). Few curves are symmetrical (Fig. 6*a*) and most of curves are asymmetrical (Fig. 6*b*, *c*), with the resistivity levels occupying larger or smaller intervals, at different numbers of representative values in the samples. The histograms for different sites differ also quantitatively: ρ magnitudes corresponding to the same levels vary in large ranges and the boundary values are different.

The reason is that, besides the geodynamic control, shallow resistivity depends on lithology and climate which affect moisture and weathering patterns and vary considerably over the area. Therefore, the ρ behavior should be analyzed separately for each site.

Generally, the degree of deformation (fracture density) in faulted rocks of the Olkhon area correlates with resistivity: the D and ρ values are in inverse exponential relationship and show qualitatively similar distributions. The values of both parameters can be divided into five levels corresponding to five levels of deformation. This empirical relationship creates a basis for a new approach to interpretation of resistivity images, but it requires theoretical substantiation proceeding from laws of faulting.

Tectonophysical approach to inversion of ERT responses of faulted crust: theoretical background and practical uses

The five deformation levels revealed in structural and ERT data from the Olkhon area may be related with zoning of faults, which are present at all sites. There are at least four levels in the model of Fig. 1*b*: one corresponding to the background rock and three others to the fault zone, with deformation degrees increasing at each faulting phase. The specific types of structural zoning and its record in the resistivity pattern are inferred from the position of fault planes and domains of different D levels within the reference fault zones. The idea and main results of modeling are discussed for the case of the Ontkhoi site (Fig. 3) used above to illustrate the division into ρ and D levels (Fig. 5*a*, *c*, *d*).

The zone-related structural patterns of faults in the Ontkhoi Cape were characterized according to the distribution of rock

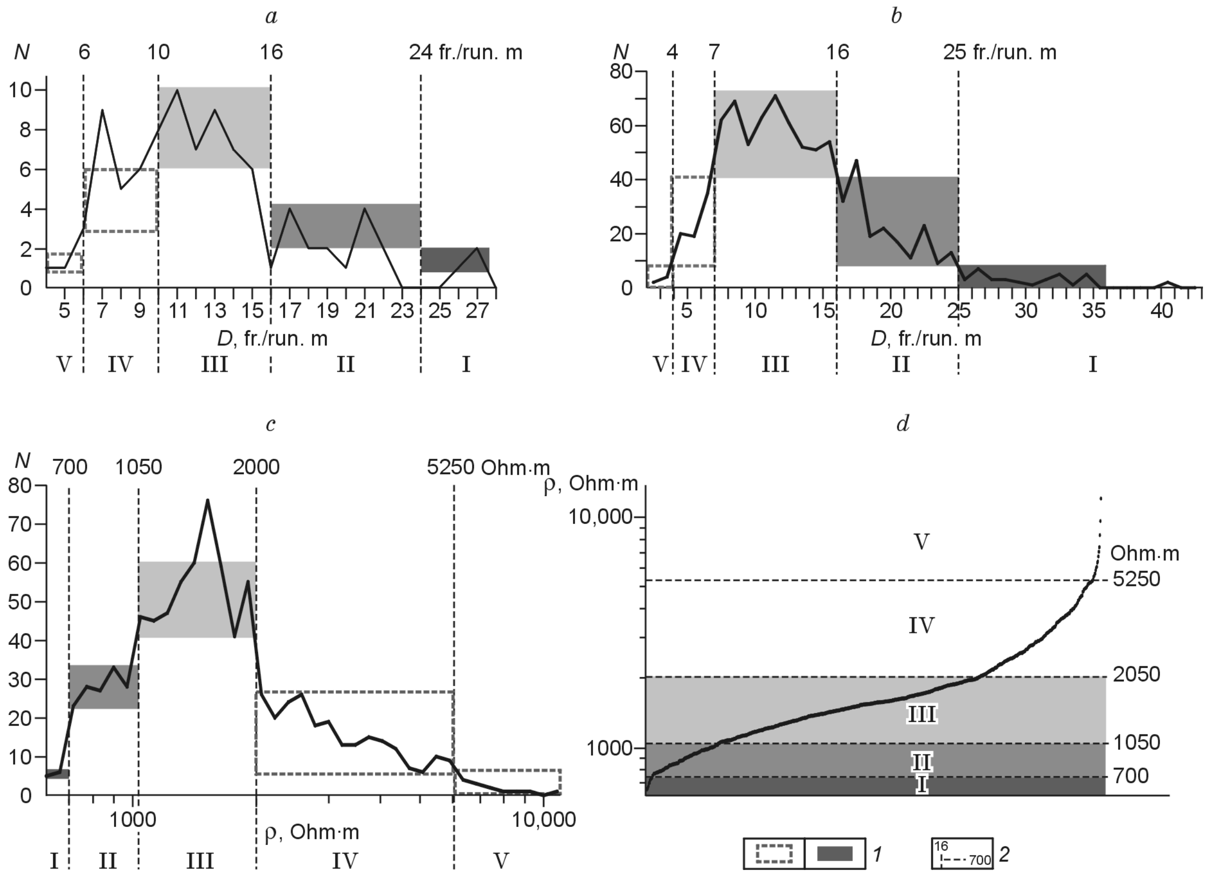

Fig. 5. Five levels of fracture density (D) and resistivity (ρ). *a*, D histogram for Ontkhoi site (No. 15); *b*, D histogram, average over three sites (Nos. 14, 15, and 19); *c*, ρ histogram for Ontkhoi site (No. 15); *d*, ρ curve, with parameter values in increasing order at equal intervals along *x* axis. *1*, curve fragments with similar frequency (N) of D or ρ values; *2*, boundaries of fragments corresponding to five (I–V) deformation states of rocks subjected to several phases of faulting, with different ranges of D and/or ρ values.

fragments with different fracture densities (number of fractures per running meter): <6 (V), 6–9 (IV), 10–15 (III), 16–23 (II), and >23 (I) (Fig. 3*c*). See Fig. 1*a* for the deformation patterns with $D = 7$, 10, 16, and 24 fractures/m. According to the locations of different fragments, correlated with the structural cross section of the cliff part accessible from the land (Fig. 3*b*), one fault plane corresponds to deformation level I and two others to level II distributed discontinuously over the profile. The leftmost fragment (level II, profile interval 22–23 m) may belong to a domain of high fracture density. Therefore, fault planes or fractured zones may also occur in domains of this deformation level which remain beyond the cross section (intervals 58–62 and 64–67 m). Like fragments of level II, those of level III are discontinuously distributed over the profile and include large fractures with minor slip or with slickensides revealed by structural data. Weakly deformed fragments ($D < 10$ fractures/m) on the profile ends enclose small stable domains of aplitic granite and migmatite with $D < 6$ fractures/m.

The uneven distribution of fracture density observed at the Ontkhoi site is common to active tectonic areas worldwide (Chernyshov, 1983; Danielsen and Dahlin, 2009; Micarelli et al., 2003). It is difficult to outline relatively homogeneous domains of blocks or faults if fragments with different fracture densities coexist within small areas. On the other hand, a large (first order) fault zone can enclose smaller (second order) stable blocks among abundant deformed rocks, or a large (first order) block can enclose smaller (second order) fault planes. Therefore, size of fragments with different deformation levels can be a formal parameter in reconstructions, with smaller fragments assumed to be parts of larger ones.

This approach was applied to the reference fault zones of the Olkhon area, separately for each fracture density level. At the Ontkhoi site, levels II, III and IV were assigned to fragments with $D \geq 16$, $D \geq 10$ and $D \geq 6$ fractures/m, as well as to intermediate intervals with D less than 16 (for II), 10 (for III), and 6 (for IV) fractures per running meter (Fig. 3*c*) which were smaller than one or both next intervals with $D \geq$ 16, 10, and 6 fractures/m, respectively (see braces in Fig. 3*c*). Therefore, the density $D = 10$ fractures/m marks the boundary of the reference fault zone, which has formed in the course of three faulting phases (I–III) and stands out against the background with the fracture density of levels IV or V (rare cases of monolith inclusions).

The structural zoning inferred for each reference site was compared with resistivity maps where contour lines were drawn as boundaries of levels I–V revealed previously from ρ histograms. The resistivity pattern of the Ontkhoi site

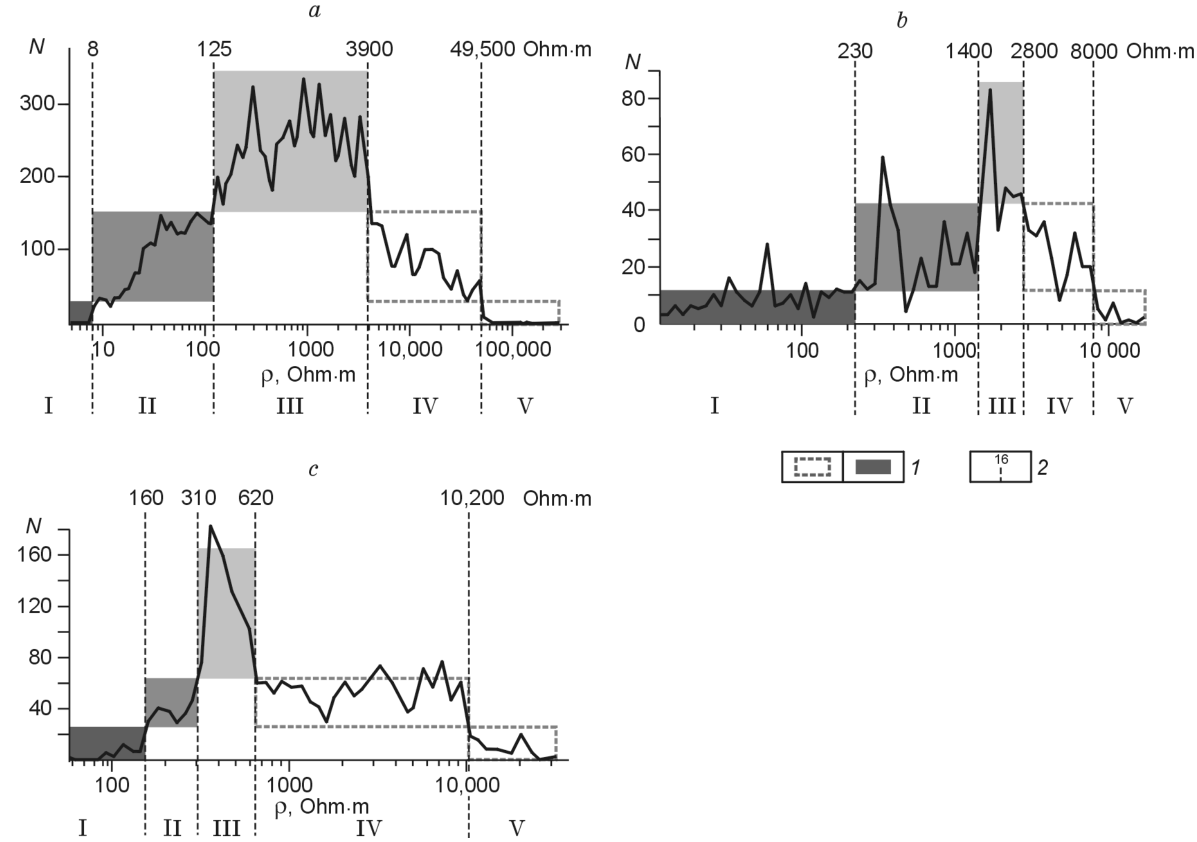

Fig. 6. ρ histograms, from ERT data at sites 20 (*a*), 14 (*b*) and 16 (*c*) typical of Olkhon area. *1*, curve fragments with similar frequency (*N*) of ρ values; *2*, boundaries of fragments corresponding to five (I–V) deformation states with different ρ ranges.

(Fig. 3*e*) matched the structure of the fault zone (Fig. 3*c*) as far as it was possible in the presence of interfering moisture effects. The key point was that the generalized boundaries coincided in the largest fracture density subzones II and III (see braces above the resistivity section). As for subzone I, the resistivity pattern included three more domains of the respective deformation degree, besides the *D*-based fragment, which spatially coincided with fault planes making the architecture of a normal fault zone (Fig. 3*c*). The largest fragment, with 345°∠60°, is beyond the structural section (Fig. 3*b*) but appears as a scarp in the photograph taken from the ice of Lake Baikal (Fig. 3*a*).

Transverse zoning of faults revealed in both resistivity and structural patterns using a common approach, as well as the correlation of the structural pattern with faulting phases, make basis for a resistivity model of deformed rocks (Fig. 7). The curve is based on the same data set as the histogram of Fig. 5*c* (ρ values arranged in an increasing order) and is similar to the curve of Fig. 5*d*, but it highlights the deformation levels in a more spectacular way. The top and base curve segments (shown by a heavy dash line restricted to few sites) separate almost undeformed and ultimately deformed rocks (no fractures, ρ of tens and hundreds of thousand Ohm·m and gouge in fault plane, ρ = 3–30 Ohm·m, respectively) from the main body of the model; the respective fracture patterns are sketched on the right (Fig. 7).

Resistivity within curve segments V and IV corresponds to the background fracture density at mostly elastic or ductile deformation, with resistivity of a few thousand of Ohm·m in the presence of micro- and macrofractures (V and IV levels, respectively). The scarce fracture network may also include nontectonic faults (some due to stresses associated with Earth's rotation). Resistivity values at level III refer to a fault zone and record deformation at the early faulting phase. This deformation level is the most widespread in active tectonic areas due to superposition of older and younger activity phases (the respective curve segments slope at a low angle). Along with the absence of large faults, this explains why structural geologists commonly classify rocks of level III as background. The fewer ρ values of level II correspond to localized deformation of a later phase, when fracture density increases and large fault planes are marked by "soft" tectonites. Low resistivity at level I is due to abundance of fault gouge and breccias produced by slip on the main fault plane and large pinnate faults at the phase of ultimate failure.

The model of Fig. 7 is a theoretical basis for the tectonophysical approach to interpretation of ERT data from active tectonic areas. In its practical application, the approach works as follows. The field work begins with choosing the location of profiles and imaging resolution according to the orientations and sizes of faults and specific objectives. In the general case, geoelectric profiles run across the fault strike transcending the limits of the damage zone expressed geomor-

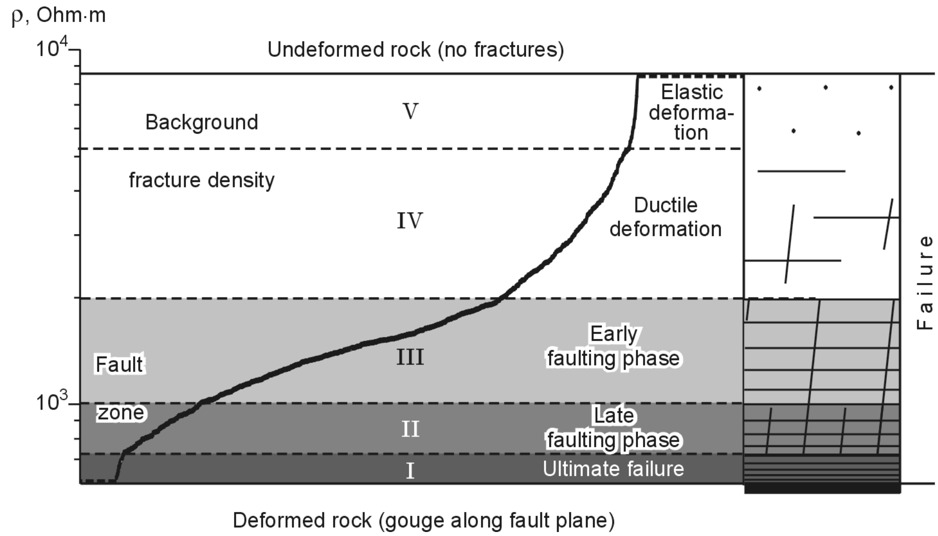

Fig. 7. Generalized curve of ρ values in increasing order, with five respective levels of deformation (I–V) within shallow crust cut by a fault zone that completed all phases of evolution. Patterns on the right are sketches of fault networks. See text for explanation.

phically as a linear depression or structurally as changes of fracture orientations in distant bedrock outcrops, etc. Acquisition and preliminary processing of resistivity data follow the standard procedures, while interpretation requires special processing. The latter procedure includes several steps: plotting frequency histograms of resistivity values; distinguishing five deformation levels on their basis; correlating the respective parts of the rock mass with the resistivity pattern; constraining the limits of the fault zone and its most strongly deformed fragments of late and final phases of faulting.

This approach was applied to ERT data from five sites in the Olkhon area (Nos. 12, 14, 16, 18, and 20) where the presence of faults was inferred from implicit signatures (Fig. 2). The fault limits and zoned structure were constrained at all sites (illustrated below by the case of site 14). The ERT profile was laid 250 m far from the cliff (Fig. 8*a*) where the main fault plane was revealed directly from structural data. Surveys by a system with electrodes spaced at 5 m (Fig. 8*b*) yielded a resistivity section to a depth of ≈40 m. The contour lines were drawn at 230, 1400, 2800, and 8000 Ohm·m assumed to be boundaries of five levels according to the resistivity histogram (Fig. 6*b*). A fault with a typical zoned structure is well evident in the cross section (Fig. 8*b*) against the background resistivity (levels IV and V). Off the fault axis, the subzone of the main fault plane (level I) gives way to that of second-order faults and high facture density (level II) and then to the peripheral subzone of genetically related fractures (level III). The subzones widen up toward the surface as a result of stress release and weathering, which imparts a characteristic "mushroom"-shaped profile to the zone, especially prominent at depths 15–20 m.

Thus, the new approach to interpretation of resistivity images has been tested and showed its efficiency in studies of shallow deformed crust to depths 40–50 m. It allowed distinguishing subzones of the main fault plane (I), second-order faults (II), and peripheral fractures (III) within sites inaccessible for direct structural measurements. The shapes and sizes of the subzones, compared to weakly deformed blocks, agree with known patterns of faulting in active tectonic areas. Note however that the conditions for ERT surveys in the Olkhon area differ notably from those in other regions where the resistivity distribution can be affected also by factors other than faulting: soft sediments, mineralization, water-filled porosity, permafrost, etc. Therefore, the reported new approach requires further testing in different areas for elaboration of its essential details.

Conclusions

Data of shallow resistivity tomography at eleven sites of faulted crust in the Olkhon area (Western Baikal region) were interpreted in terms of tectonophysical laws of faulting, which led to the following inferences.

1. The resistivity patterns of shallow bedrock in the studied active tectonic area are controlled by patterns of faults of different ranks (sizes). The general trend is exponential decrease of resistivity (ρ) with increasing density of fractures (*D*), with ρ and *D* varying in certain ranges corresponding to five levels of deformation. Histograms of the two parameters show that this correlation appears at almost all sites qualitatively (the same number of levels) though its quantitative expression (values of parameters at different levels) differs according to specific geological, landscape and climate conditions.

2. Analysis of resistivity maps along profiles that cross reference faults in the Olkhon area, studied previously by structural methods, allowed us to correlate resistivity and deformation levels. Namely, levels V and IV of high resistivity (low conductivity) are typical of small monolith blocks or rocks with a background fracture density outside fault zones, while levels I–III of low resistivity represent fault zones in a

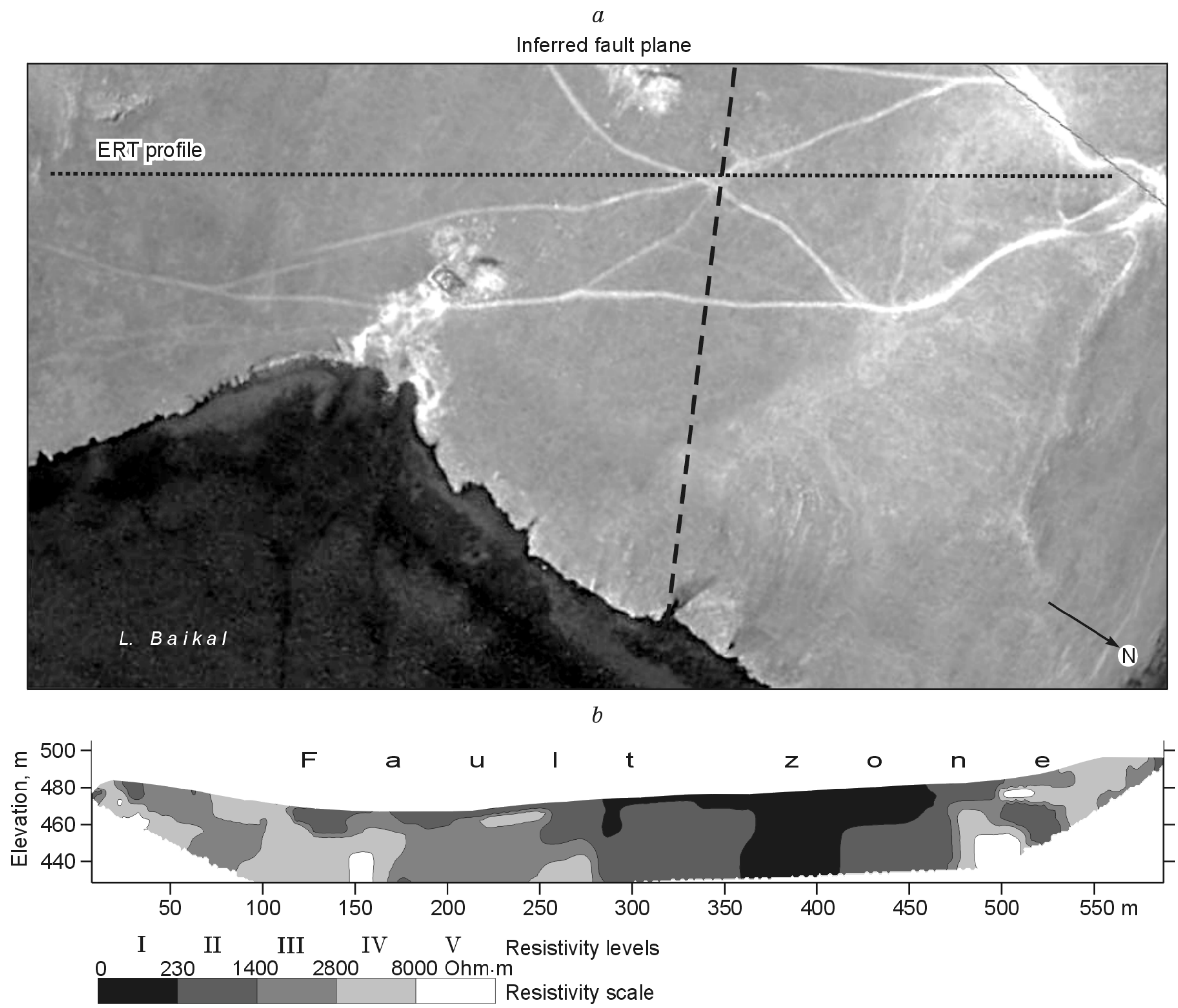

Fig. 8. A buried fault in a satellite image at site 14 (*a*) and in a resistivity (ERT) cross section (*b*) interpreted using the new tectonophysical approach. Contour lines divide section fragments corresponding to five (I–V) deformation levels revealed from ρ histogram.

broad tectonophysical sense, with subzones of the main fault plane near the axis (I) and secondary pinnate faults and high fracture density (II) surrounded on the periphery by broad subzones of genetically related fractures (III).

3. The revealed structural zoning creates a basis for the new approach to interpretation of shallow resistivity images for detection of faults in areas where setting up direct structural measurements is hard or impossible. The approach is quite well formalized, and the respective interpretation procedure consists of several steps: plotting frequency histograms of resistivity values; distinguishing five deformation levels on their basis; correlating the respective parts of the rock mass with the resistivity pattern; constraining the limits of the fault zone and its most strongly deformed fragments of late and final phases of faulting (subzones I and II). The information thus obtained has many theoretical and applied uses in tectonics, metallogeny, and engineering geology.

The new approach to interpretation of ERT data has shown its efficiency in studies of buried faults in the Olkhon area and requires further testing in other regions.

We wish to thank A.V. Cheremnykh and A.A. Bobrov, as well as Yu.P. Burzunova and A.S. Cheremnykh, our colleagues from the Laboratory of tectonophysics at the Institute of the Earth's Crust in Irkutsk, for assistance in acquisition and processing of field data. We greatly appreciate valuable advice and criticism by M.I. Epov during the manuscript preparation.

The study was partly supported by grant 16-05-00154 from the Russian Foundation for Basic Research.

References

Bobachev, A.A., Marchenko, M.N., Modin, I.N., Pervago, E.V., Urusova, A.V., Shevnin, V.A., 1995. Geoelectrical imaging of laterally heterogeneous media: New approaches. Izv. RAN, Fizika Zemli, No. 12, 79–90.

Carbonel, D., Gutiérrez, F., Linares, R., Roqué, C., Zarroca, M., McCalpin, J., Guerrero, J., Rodríguez, V., 2013. Differentiating between gravitational and tectonic faults by means of geomorphological mapping, trenching and geophysical surveys. The case of the Zenzano Fault (Iberian Chain, N Spain). Geomorphology 189, 93–108.

Chernyshev, S.N., 1983. Fractures in Rocks [in Russian]. Nauka, Moscow.

Danielsen, B.E., Dahlin, T., 2009. Comparison of geoelectrical imaging and tunnel documentation at the Hallandsas Tunnel, Sweden. Eng. Geol. 107, 118–129.

Delvaux, D., Moyes, R., Stapel, G., Melnikov, A., Ermikov, V., 1995. Paleostress reconstruction and geodynamics of the Baikal region, Central Asia. Part I: Palaeozoic and Mesozoic pre-rift evolution. Tectonophysics 252, 61–101.

Delvaux, D., Moyes, R., Stapel, G., Petit, C., Levi, K., Miroshnitchenko, A., Ruzhich, V., San'kov, V., 1997. Paleostress reconstruction and geodynamics of the Baikal region, Central Asia. Part II: Cenozoic rifting. Tectonophysics 282, 1–38.

Favorskaya, M.A., Volchanskaya, I.K., Sapozhnikova, E.N., Vinogradov, I.V., Kurchavov, A.M., Baskina, V.A., Shilin, N.L., 1985. Fault Systems: Tectonics, Magmatism, and Metallogeny [in Russian]. Nauka, Moscow.

Ganerod, G.V., Ronning, J.S., Dalsegg, E., Elvebak, H., Holmoy, K., Nilsen, B., Braathen, A., 2006. Comparison of geophysical methods for sub-surface mapping of faults and fracture zones in a section of the Viggja road tunnel, Norway. Bull. Eng. Geol. Environ. 65, 231–243.

Griffiths, D.H., Barker, R.D., 1993. Two-dimensional resistivity imaging and modelling in areas of complex geology. J. Appl. Geophys. 29, 211–226.

Gubatenko, V.P., Ogadzhanov, V.A., Nazarov, A.A., 2000. Resistivity surveys for monitoring of rock density. Izv. RAN, Fizika Zemli, No. 9, 103–109.

Gzovsky, M.V., 1975. Fundamentals of Tectonophysics [in Russian]. Nauka, Moscow.

Improta, L., Ferranti, L., De Martini, P.M., Piscitelli, S., Bruno, P.P., Burrato, P., Civico, R., Giocoli, A., Iorio, M., D'Addezio, G., Maschio, L., 2010. Detecting young, slow-slipping active faults by geologic and multidisciplinary high-resolution geophysical investigations: A case study from the Apennine seismic belt, Italy. J. Geophys. Res. 115, B11307. doi:10.1029/ 2010JB000871.

Khrenov, P.M., 1971. Buried faults in orogenic and platform areas (a case study of East Siberia), in: Khrenov, P.M. (Ed.), Deep Faults in Southern East Siberia and Their Role in Metallogeny [in Russian]. Nauka, Moscow, pp. 5–38.

Kozhevnikov, N.O., 1998. Structural peculiarities of the Ol'khon region according to electrical prospecting data. Geologiya i Geofizika (Russian Geology and Geophysics) 39 (2), 271–276 (279–284).

Kuria, Z.N., Woldai, T., van der Meer, F.D., Barongo, J.O., 2010. Active fault segments as potential earthquake sources: Inferences from integrated geophysical mapping of the Magadi fault system, southern Kenya Rift. J. African Earth Sci. 57, 345–359.

Levi, K.G., Arzhannikova, A.V., Buddo, V.Yu., Kirillov, P.G., Lukhnev, A.V., Miroshnichenko, A.I., Ruzhich, V.V., Sankov, V.A., 1997. Modern geodynamics of Baikal rift. Razvedka i Okhrana Nedr, No. 1, 10–20.

Logatchev, N.A., 2003. History and geodynamics of the Baikal rift. Geologiya i Geofizika (Russian Geology and Geophysics) 44 (5), 91–106 (391–406).

Loke, M.H., 2010. Tutorial: RES2DINV version 3.59, Rapid 2-D Resistivity & IP Inversion Using the Least-Squares Method. Malaysia. Geotomo Software.

Magnusson, M., Fernlund, J., Dahlin, T., 2010. Geoelectrical imaging in the interpretation of geological conditions affecting quarry operations. Bull. Eng. Geol. Environ. 3, 465–486.

Makarov, V.I., Shchukin, Yu.K., 1979. Estimating activity of buried faults. Geotektonika, No. 1, 96-109.

Makrygina, V.A., Tolmacheva, E.V., Lepekhina, E.N., 2014. Crystallization history of Paleozoic granitoids in the Ol'khon region, Lake Baikal (SHRIMP-II zircon dating). Russian Geology and Geophysics (Geologiya i Geofizika) 55 (1), 33–45 (41–55).

Mats, V.D., 1993. The structure and development of the Baikal rift depression. Earth Sci. Rev. 34, 81–118.

Micarelli, L., Moretti, I., Daniel, J.M., 2003. Structural properties of rift-related normal faults: the case study of the Gulf of Corinth, Greece. J. Geodyn. 36, 275–303.

Nikolaev, P.N., 1992. Methods of Tectonophysical Analysis [in Russian]. Nedra, Moscow.

Olenchenko, V.V., Kamnev, Ya.K., 2014. A resistivity model of permafrost in the Zhosaly Kezen Pass (Ilei Alatau), from ERT data, in: Proc. Geo-Siberia Int. Conf. & Expo, Vol. 2 (2), pp. 1–5.

Peive, A.V. (Ed.), 1990. Deep Faults and Their Role in the Crust Structure and Evolution. Selected Works [in Russian]. Nauka, Moscow.

Radkevich, E.A., Tomson, I.N., Gorlov, N.V., 1956. Regional-scale fracture zones. Sovetskaya Geologiya 58, 170–185.

Rats, M.V., Chernyshev, S.N., 1970. Fractures and Properties of Fractured Rocks [in Russian]. Moscow, Nedra.

Reiser, F., Dalsegg, E., Dahlin, T., Ganerod, G.V., Ronning, J.S., 2009. Resistivity modelling of fracture zones and horizontal layers in bedrock. Geol. Survey Norway, Report No. 2009.070.

Ronning, J.S., Ganerod, G.V., Dalsegg, E., Reiser, F., 2014. Resistivity mapping as a tool for identification and characterisation of weakness zones in crystalline bedrock: definition and testing of an interpretational model. Bull. Eng. Geol. Environ. 73, 1225–1244.

Ryazantsev, P.A., 2012. A composite geophysical profile across the Ropruchei gabbro-dolerite sill in the Rzhanoye–Anashkino area. Transactions of Karelian Science Center, No. 3, 165–171.

Schutze, C., Vienken, T., Werban, U., Dietrich, P., Finizola, A., Leven, C., 2012. Joint application of geophysical methods and Direct Push-soil gas survey for the improved delineation of buried fault zones. J. Appl. Geophys. 82, 129–136.

Seminsky, K.Zh., 2003. Inner Structure of Continental Fault Zones: Tectonophysical Aspect [in Russian]. Izd. SO RAN, Filial "Geo," Novosibirsk.

Seminsky, K.Zh., 2005. Mapping the structure of faulted crust in terms of tectonophysics. Geofizicheskii Zhurnal 27 (1), 85–96.

Seminsky, K.Zh., 2014. Special mapping of crustal faults. Article 1: Theoretical principles. Geodinamika i Tektonofizika 5 (2), 445–467.

Seminsky, K.Zh., Kozhevnikov, N.O., Cheremnykh, A.V., Pospeeva, E.V., Bobrov, A.A., Olenchenko, V.V., Tugarina, M.A., Potapov, V.V., Zaripov, R.M., Cheremnykh, A.S., 2013. Fault boundaries in the crust of southern East Siberia: Tectonophysical interpretation of geological and geophysical data. Geodinamika i Tektonofizika 4 (3), 203–278.

Sherman, S.I., Seminsky, K.Zh., Bornyakov, S.A., Adamovich, A.N., Lobatskaya, R.M., Lysak, S.V., Levi, K.G., 1992. Faulting in the Lithosphere. Zones of Extension [in Russian]. Nauka, Novosibirsk.

Sherman, S.I., Seminsky, K.Zh., Bornyakov, S.A., Adamovich, A.N., Lobatskaya, R.M., Lysak, S.V., Levi, K.G., 1994. Faulting in the Lithosphere. Zones of Compression [in Russian]. Nauka, Novosibirsk.

Sklyarov, E.V. (Ed.), 2005. Structural and Tectonic Correlation across the Central Asia Orogenic Collage: North-Eastern Segment (Guidebook and Abstract Volume of the Siberian Workshop IGCP-480). IES SB RAS, Irkutsk.

Sokolov, S.Ya., Ryazantsev, P.A., Klimovsky, A.V., Nilov, M.Yu., 2011. Geophysical studies in quarries of ornamental stones. Gornyi Zhurnal, No. 5, 15–19.

Zamaraev, S.M., Vasiliev, E.P., Mazukabzov, A.M., Ruzhich, V.V., Ryazanov, G.V. (Eds.), 1979. Relations of Pre-Cenozoic and Cenozoic Structures in the Baikal Rift Zone [in Russian]. Novosibirsk, Nauka.

Zaripov, R.M., 2013. Electrical Resistivity Tomography for studies of faults in the Olkhon area (Western Baikal region), in: Epov, M.I. (Ed.), Proc. Conf. Andrei Trofimuk Readings-2013 [in Russian]. INGG, Novosibirsk, pp. 271–274.

Editorial responsibility: M.I. Epov